A model-based ¹³C-sucrose breath test diagnostic for gut function disorders characterized by a loss of sucrase-isomaltase enzymatic activity

Andrew F. Brouwer^{1,*}, Gwenyth O. Lee², Hannah Van Wyk¹, Robert J. Schillinger^{3,4}, Christine A. Edwards⁴, Douglas J. Morrison³

Abstract

- 1 Background: Environmental enteric dysfunction (EED) causes malnutrition in children in low-
- 2 resource settings. Stable isotope breath tests have been proposed as non-invasive tests of altered
- 3 nutrient metabolism and absorption in EED, but uncertainty over interpreting the breath curves has
- 4 limited their use. The activity of sucrase-isomaltase, the glucosidase enzyme responsible for
- 5 sucrose hydrolysis, may be reduced in EED. We previously developed a mechanistic model
- describing the dynamics of the ¹³C-sucrose breath test (¹³C-SBT) as a function of underlying
- 7 metabolic processes.
- 8 **Objective:** 1) To determine which breath test curve dynamics are associated with sucrose
- 9 hydrolysis and with the transport and metabolism of the fructose and glucose moieties, and 2) to
- propose and evaluate a model-based diagnostic for the loss of activity of sucrase-isomaltase.
- 11 **Methods:** We applied the mechanistic model to two sets of exploratory ¹³C-SBT experiments in
- healthy adult participants. First, 19 participants received differently labeled sucrose tracers (U-¹³C

¹ Department of Epidemiology, University of Michigan, 1415 Washington Heights, Ann Arbor, 48109, MI, United States.

² Rutgers Global Health Institute, Rutgers University, 112 Paterson St. New Brunswick, NJ 08901

³ Scottish Universities Environmental Research Centre, University of Glasgow, Rankine Avenue, East Kilbride, G75 0QF, United Kingdom.

⁴ School of Medicine, Dentistry and Nursing, University of Glasgow, University Ave, Glasgow, G12 8QQ, United Kingdom.

^{*} Correspondence: Andrew F. Brouwer, brouweaf@umich.edu

fructose, U-¹³C glucose, and U-¹³C sucrose) in a cross-over study. Second, 16 participants received

a sucrose tracer accompanied by 0 mg, 100 mg, and 750 mg of Reducose®, a sucrase-isomaltase

inhibitor. We evaluated a model-based diagnostic distinguishing between inhibitor concentrations

using receiver operator curves, comparing to conventional statistics.

17 **Results:** Sucrose hydrolysis and the transport and metabolism of the fructose and glucose moieties

were reflected in the same mechanistic process. The model distinguishes these processes from the

fraction of tracer exhaled and an exponential metabolic process. The model-based diagnostic

performed as well as the conventional summary statistics in distinguishing between no and low

inhibition (AUC 0.77 vs 0.66–0.79) and for low vs high inhibition (AUC 0.92 vs 0.91–0.99).

22 **Conclusions:** Current summary approaches to interpreting ¹³C breath test curves may be limited

to identifying only gross gut dysfunction. A mechanistic model-based approach improved

interpretation of breath test curves characterizing sucrose metabolism.

Abbreviations:

EED: environmental enteric dysfunction

SI: sucrase-isomaltase

MLE: mulberry leaf extract SBT: sucrose breath test

ROC: receiver operator curve AUC: area under the curve

25

26

14

15

16

18

19

20

21

23

24

Keywords: environmental enteric dysfunction; breath test; ¹³C; stable isotope; mechanistic model;

27 sucrose; fructose; glucose; Reducose; mulberry leaf extract

Introduction

28

29

30

31

32

33

34

35

36

37

38

39

40

41

42

43

44

Gut dysfunction disorders causing nutrient maldigestion and malabsorption, including environmental enteropathy or environmental enteric dysfunction (EED)(1,2), have a substantial burden worldwide. EED is characterized by small intestinal villous atrophy, where the villi are blunted, reducing the capacity for nutrient absorption; this blunting is accompanied by gut barrier disruption and intestinal inflammation (3,4). Essential nutrient malabsorption and chronic inflammation lead to changes in nutrient supply and demand that may be exacerbated by marginal nutrition, limiting availability of nutrients to support linear growth and leading to stunting in children (5). High pathogen burdens may contribute to the prevalence of EED, which is thought to be highly prevalent among the 2 billion people in low-resource settings that lack adequate access to water and sanitation (6). Diagnosis of EED is limited by the lack of a reliable, non-invasive test to assess intestinal damage. The 'gold standard' diagnoses for environmental enteropathy requires identification of histologic changes to the small intestine through biopsy, which is invasive and impractical and creates ethical challenges, particularly in resource-constrained settings (7). While non-invasive tests exist, they have substantial limitations. For EED, the most widely accepted noninvasive test (the lactulose:rhamnose ratio test) is time-consuming to administer and inconsistent across laboratory platforms (8) and is accordingly used only for research. To overcome these limitations, there have been calls for the development of tests to assess

- 45
- functional changes in the small intestine resulting from EED (9). Disaccharide metabolism has 46
- 47 been identified as a target for such a test because sucrase-isomaltase (SI), an intestinal
- glucosidase enzyme responsible for sucrose hydrolysis, is secreted at the intestinal brush border, 48
- 49 which is compromised by villus atrophy (10,11). Indeed disruption of sucrose metabolism has
- been identified in both EED (12) and in coeliac disease and other disorders with functional 50

similarities (13–16). The ¹³C-sucrose breath test (¹³C-SBT) is a stable-isotope breath test 51 intended to assess SI activity non-invasively. The test provides a dose of non-radioactive ¹³C-52 labeled sucrose tracer, which is digested by SI (into fructose and glucose) and metabolized, 53 ultimately appearing on the breath as ¹³CO₂. Slower recovery of the tracer on the breath indicates 54 reduced metabolic function. 55 However, the ¹³C-SBT is also limited as a test of intestinal function insofar as the ¹³CO₂ breath 56 signal (serial measurements over time) integrates multiple metabolic processes. Although the 57 tracer and its labeling pattern are chosen such that the target function (substrate hydrolysis and 58 absorption) is the rate-limiting step, the final, observed signal may be influenced not only by this 59 process but also by downstream metabolism and bicarbonate kinetics. This limitation is not 60 unique to the ¹³C-SBT and is common to many stable isotope breath tests. 61 Hence, the potential clinical impact of ¹³C-SBT and other stable isotope breath tests has thus far 62

Hence, the potential clinical impact of ¹³C-SBT and other stable isotope breath tests has thus far been limited by a lack of clarity about how to interpret the resulting breath curve. In our previous work (17), we used a mechanistic model of sucrase metabolism to link ¹³C-SBT curves to parameters representing underlying metabolic rates. However, because the previous data did not include participants with real or induced loss of SI activity and only used a uniformly labeled sucrose tracer, we were not able to determine which model parameters were associated with which biological processes. In this analysis, we fit our mechanistic model to multiple additional ¹³C-SBT experiments to develop and evaluate a model-based diagnostic for a loss of SI activity.

Methods

63

64

65

66

67

68

69

70

71

Overview

This analysis used data from two sets of exploratory ¹³C-SBT experiments. In the first set of experiments, participants were given a sucrose tracer for which the isotope label was present i) only on the fructose moiety (U-13C fructose), ii) only to the glucose moiety (U-13C glucose), and iii) to both moieties (U-13C sucrose). In these experiments, the primary outcome was the percent dose recovery rate (described below) at each time point. The analyses in this work are post-hoc analyses and are thus considered exploratory. Specficially, we leveraged these data to determine whether differences in fructose and glucose transport and metabolism impact ¹³C-SBT breath curves and whether these differences need to be accounted for when interpreting curves from a uniformly labeled sucrose tracer. In the second set of experiments, participants were given a uniformly labeled sucrose tracer alongside 0, 100, and 750 mg of mulberry leaf extract (MLE, proprietary name Reducose®), an SI inhibitor (18). This set of experiments was designed to approximate the reduction of SI activity in individuals with gut dysfunction. We leveraged these data to determine which mechanistic model parameter(s) were impacted by the reduction in SI activity, to develop a model-based ¹³C-SBT diagnostic for reduced SI activity, and to compare the diagnostic to other common ¹³C-SBT summary measures. The data, model, and analysis plan are discussed in more detail below.

Data

72

73

74

75

76

77

78

79

80

81

82

83

84

85

86

87

88

89

90

91

92

93

94

General information. Adult participants for ¹³C-SBT experiments were recruited by advertisement in the Glasgow area, were between the ages of 18–35 years, and had no history of gastrointestinal symptoms or disease. Participants gave informed consent, and the studies were approved by the University of Glasgow College of Medical, Veterinary & Life Sciences Research Ethics Committee (Application Numbers: 200190014 and 200190155). Each participant was instructed to follow a low ¹³C diet (i.e., a diet low in food derived from C₄ plants such as corn or

cane sugar) for three days and to fast for eight hours prior to testing (19). Participants continued to fast for 4 hour tests but were fed a low ¹³C lunch at 4 hours for tests lasting longer than 4 hours. Previous work has shown that this meal can influence curve dynamics after 5 hours when using a naturally enhanced (0.016 atom% excess) tracer but not with not the highly enhanced (≥99 atom% excess) tracer used here (20). Physical activity was restricted during the test (participants were sedentary).

At the beginning of the experiment, participants were given a dose of sucrose tracer dissolved in 100 mL of water. See the experimental details below for the dose and isotopic labeling specifications for each experiment. A baseline breath sample was collected immediately prior to the participant ingesting the tracer. Breath samples were then taken every 15 min for four to eight hours, depending on the specific experiment. Samples were collected in 12 mL Exetainer breath-sampling vials (Labco, United Kingdom) and analyzed by isotope ratio mass spectrometry (IRMS AP-2003, Manchester, United Kingdom). Isotope abundance in the samples was measured as δ^{13} C (in ‰), defined as the relative difference in parts per thousand between the ratio $R_s = [^{13}\text{C}]/[^{12}\text{C}]$ in the sample and international calibration standard R = 0.0112372 (21). A value of δ^{13} C was converted into isotope abundance A (in ppm) as

111
$$A = 10^6 / \left(1 + 1 / \left(R \cdot \left(1 + \frac{\delta^{13} C}{1000} \right) \right) \right). \tag{1}$$

The derivation of this formula is given in Eq (4) in Brouwer et al. (17). We accounted for variation in baseline δ^{13} C varied among participants because of dietary factors by analyzing the difference between the isotope abundance at time t and at baseline, A(t) - A(0). The quantity $(A(t) - A(0))/10^6$ is the instantaneously measured excess atom fraction ¹³C. We estimated each

participant's CO_2 production (V_{CO_2} , in mmol/hr) based on their sex, body surface area, and sedentary physical activity level (22). The percent dose recovery rate (PDRr, in 1/hr) is

118
$$PDRr(t) = 100 \cdot \frac{V_{CO_2}(\text{mmol/hr}) \cdot (A(t) - A(0)) / 10^6}{\text{dose}^{13}C \text{ (mmol)}}.$$
 (2)

Sucrose moiety labeling. Nineteen healthy adults were recruited for a cross-over study consisting of three ¹³C-SBT experiments in a randomized order at least one week apart. In each of the three ¹³C-SBT experiments, the isotopic labeling of the 50 mg sucrose tracer was different. In the first experiment, the sucrose consisted of a highly (i.e., ≥99 atom%) and uniformly (i.e., no preferential ¹³C placement) enriched fructose moiety (U-¹³C fructose; 0.84 mmol ¹³C) with an unlabeled glucose moiety; in the second experiment, the sucrose consisted of a highly and uniformly enriched glucose moiety (U-¹³C glucose; 0.84 mmol ¹³C) with an unlabeled fructose moiety; in the last experiment, the sucrose was highly and uniformly enriched (U-¹³C sucrose; 1.67 mmol ¹³C). All tracers were ≥99 atom% enriched for the specified moiety (Sigma-Aldrich, Poole, United Kingdom).

Sucrase-isomaltase inhibition. Eighteen healthy adults were recruited for a stepped-dose, cross-over study consisting of a set of three 13 C-SBT experiments conducted at least one week apart. In each of the three experiments, participant were given a 25 mg dose (0.84 mmol 13 C) of U- 13 C sucrose tracer (\geq 99 atom% enriched, Sigma-Aldrich, Poole, United Kingdom). In addition to the sucrose tracer, participants were given a dose of mulberry leaf extract, Reducose® (Phynova Group Ltd., Oxford, UK), standardized to contain 5% 1-Deoxynojirimycin, which is an α-glucosidase inhibitor. The mulberry leaf extract (MLE) doses were 0 mg, 100 mg, and 750 mg for the three experiments. The MLE doses were chosen based on the recommended dose by the

manufacturer to achieve approximately 50% inhibition (750 mg, based on plasma glucose appearance in previous work (23)) and a lower dose (100 mg) intended to assess the sensitivity of the test to detect the relatively small changes in breath ¹³C output observed previously using ¹³C-SBT in an Aboriginal population (12). We only include data from the sixteen participants who completed all three experiments. For some participants, the sucrose tracer entered the colon and was metabolized by colonic bacteria, leading to a spike in the PDRr; these points are excluded from analysis.

Mechanistic Model

Description. We previously developed a mechanistic model of sucrose transport, metabolism, and excretion and determined a practically identifiable set of model parameters (i.e., a set of model parameters that can be uniquely estimated from breath curve data) that describe ¹³C-SBT breath curve dynamics (17). We found that ¹³C-SBT breath curves can be approximated by a gamma-distributed process (rate parameter ρ and shape parameter 2), an exponentially distributed process (rate parameter $\pi\rho$, where $0 < \pi \le 1$), and κ , the fraction of ¹³C that is exhaled instead of sequestered or excreted through urine. When $\pi \ne 1$, this model has the closed form expression for PDRr,

154
$$y(t) = \frac{100\kappa\pi\rho}{(1-\pi)^2} \left(e^{-\pi\rho t} + ((\pi-1)\rho t - 1)e^{-\rho t}\right),\tag{3}$$

and CPDR,

155
$$Y(t) = 100\kappa \left(1 - \frac{e^{-\pi\rho t} + ((\pi - 1)\rho t + \pi - 2)\pi e^{-\rho t}}{(1 - \pi)^2}\right). \tag{4}$$

The three parameters ρ , $\pi\rho$, and κ collectively explain the dynamics of a ¹³C-SBT breath curve. Parameter κ is a function of the relative rates of exhalation, sequestration, and non-pulmonary excretion. However, it is not known which underlying processes or collection of processes (transport, hydrolysis, exhalation, etc.) are captured in the two mathematical processes represented by ρ and $\pi\rho$.

We fit the model to data from a breath curve $\{(t_i, z_i)\}$ by minimizing the normal negative loglikelihood (NLL) as a function of the parameters,

$$NLL(\rho, \pi\rho, \kappa) = \frac{n}{2}\log(2\bar{\pi}) + \frac{n}{2}\log(\sigma^2) + \frac{1}{2\sigma^2}\sum_{i}(y(\rho, \pi\rho, \kappa; t_i) - z_i)^2,$$
 (5)

where $\bar{\pi}$ is the mathematical circle constant, n is the number of data points, t_i is the time at which measurement z_i was taken, and the standard deviation σ was estimated to be 0.555 based on deviation from best-fit curves.

Application to new experiments. Fructose and glucose are transported across the apical membrane of the enterocyte by different transporters but are transported across the basolateral membrane by the same transporter (reviewed comprehensively in Ferraris et al. (24)). Once absorbed, glucose and fructose are sequestrated into liver metabolism under differential regulatory control and are therefore oxidized at different rates. Thus, we expected to find systematic differences in ¹³C-SBT different breath curves and the underlying model parameters (25). As part of the analysis of the fructose- and glucose-labeled sucrose tracers, we considered an extension of the model in which a breath curve based on a uniformly labeled sucrose tracer is treated as the sum of two curves representing the fructose and glucose moieties:

176
$$y(t) = \frac{1}{2}y(t; \rho_F, \pi_F \rho_F, \kappa_F) + \frac{1}{2}y(t; \rho_G, \pi_G \rho_G, \kappa_G)$$
 (6)

177 A schematic of the model accounting for the possibility of separate rates of fructose and glucose 178 transport and metabolism is given in **Figure 1**A.

In the experiments with high doses of MLE, participants' breath curves may not attain their peak within the breath test experimental period, and in those cases, parameters $\pi\rho$ and κ are not identifiable. To fit this set of breath test curves, we added a penalty of the size of κ to the negative log-likelihood, which selects for the smallest of the possible values of κ and the largest of the possible values of $\pi\rho$. Under this assumption, projected breath curves would decrease as quickly as possible while still being consistent with the data, as opposed to extending as long as possible.

Data, example code, and guidance for the implementation of this model is available at: https://doi.org/10.5281/zenodo.8387995.

Analysis Plan

Comparison of model parameters in unconstrained models. We first fit the mechanistic model (Eqn 1) to each breath curve in each experiment, comparing the model parameters by fructose-vs glucose-labeled moiety and by dose of MLE in pairwise paired t-tests and repeated measures ANOVA. Then, by fitting the mechanistic model to the experimental breath curves under different sets of assumptions, we aimed to 1) interpret the model parameters in terms of the underlying biology and 2) develop a model-based diagnostic for a loss of SI activity.

Model assumptions and interpretation of model parameters. We used the following analysis plan for this objective, each step building on the results of the previous step. A graphical representation of the analysis plan is given in Figure 1B.

194

195

196

197

198

199

200

201

202

203

204

205

206

207

208

209

210

211

212

213

214

215

Step 1. Which parameter(s) reflect fructose and glucose transport and metabolism? This step evaluates whether any of the model parameters can be assumed to not be different between the fructose- and glucose-labeled breath curves using fructose- and glucose-labeled tracer experiments. We simultaneously fit the mechanistic model to each participant's breath test curves with the fructose-labeled sucrose tracer and the glucose-labeled sucrose tracer under each of seven assumptions: i) the gamma-distributed process is different ($\rho_F \neq \rho_G$, $\pi_F \rho_F = \pi_G \rho_G$, $\kappa_F = \kappa_G$); ii) the exponentially distributed process is different ($\rho_F = \rho_G$, $\pi_F \rho_F \neq \pi_G \rho_G$, $\kappa_F = \kappa_G$); iii) the exhalation fraction is different ($\rho_F = \rho_G$, $\pi_F \rho_F = \pi_G \rho_G$, $\kappa_F \neq \kappa_G$); iv) only the exhalation fraction is the same $(\rho_F \neq \rho_G, \pi_F \rho_F \neq \pi_G \rho_G, \kappa_F = \kappa_G)$; v) only the exponentially distributed process is the same $(\rho_F \neq \rho_G, \pi_F \rho_F = \pi_G \rho_G, \kappa_F \neq \kappa_G)$, vi) only the gamma-distributed process is the same $\pi_G \rho_G$, $\kappa_F \neq \kappa_G$). We used the Schwarz Information Criterion (SIC), which accounts for both the model fit to the data and the number of model parameters, to inform a choice of model assumptions. Because statistical significance does not always translate to meaningful difference, we treated the SIC results as advisory in this and subsequent steps. The model assumptions determined in Step 1 were carried forward in the analysis.

Step 2. How much does accounting for differences in fructose and glucose transport improve the model? We determined whether uniformly labeled sucrose breath curves could be modeled using the 3-parameter model (Eqn 3), or whether they should be modeled treating the curve as the sum

of two moiety-specific curves (Eqn 6), incorporating the assumptions identified in Step 1. Using the uniformly labeled sucrose breath curve from the first set of experiments, we compared the two models using the Schwarz Information Criterion (SIC). The choice of model in Step 2 determined the model used in the rest of the analysis.

Step 3. Which parameter(s) reflect sucrase-isomaltase activity? We determined which model parameter(s) were associated with sucrose hydrolysis in the small intestine. We used the data from the second set of experiments. MLE inhibits SI activity, so we expected to find systematic differences in 13 C-SBT different breath curves and thus associate the process of sucrose hydrolysis with one or more model parameters. We applied the model identified in Step 3 to each of the curves, and we also assessed whether the $\pi\rho$ parameter could be considered the same across the curves (see results of Step 1, below). We used the Schwarz Information Criterion (SIC) to compare model fits and parsimony and to inform a choice of final model assumptions.

Development of a model-based ¹³C-SBT diagnostic. How does a model-based diagnostic compare to convention summary statistics? Based on the results of the analyses above, we proposed a model-based ¹³C-SBT diagnostic and used receiver operator curves to determine optimal thresholds for distinguishing between the breath curves with 0 mg of MLE vs. 100 or 750 mg of MLE (no vs. low or high inhibition) and between 0 or 100 mg of MLE vs 750 mg of MLE (no or low vs. high inhibition). Using the area under the curve (AUC), we compared the model-based ¹³C-SBT diagnostic to four breath curve summary measures: cumulative percent dose recovered at 90 minutes (cPDR90), peak PDRr, time to peak PDRr, and time to recovery of 50% of the dose (50% cPDR).

Results

- Participant characteristics. Participant characteristics are summarized in Table 1.
- 239 Comparison of model parameters in unconstrained models. When fitting the mechanistic model
- 240 to the fructose-labeled sucrose tracer and the glucose-labeled sucrose tracer breath curves
- separately (Figure 2, top row), all three parameters were statistically significantly different
- between the two experiments (ρ : p=0.002; $\pi\rho$: p=0.015, and κ : p=0.042). The greatest differences
- 243 were observed in ρ .

238

- 244 When fitting the mechanistic model to the MLE experiments separately (Figure 2, bottom row),
- parameter ρ was again the most different between the curves, with a clear suppression of values
- 246 with increased dose of MLE (0 vs 100 mg: p=0.09; 100 vs 750 mg: p=<0.001; 0 vs 750 mg:
- p=<0.001; ANOVA: p=<0.001). Parameter $\pi\rho$ was not significantly different across the MLE
- 248 concentrations (ANOVA: p=0.56). Parameter κ differed across the experiments (ANOVA: p
- 249 <0.001) but in the pairwaise comparisons only differed between the 750 mg curve and each of the</p>
- other curves. Note, however, that $\pi \rho$ and κ were not identifiable for most of the 750 mg curves
- and that these values represent the smallest values of κ and largest values of $\pi \rho$ that could still fit
- 252 the data; thus the results for $\pi \rho$ and κ for the 750 mg curves should be treated with caution.
- 253 Model assumptions and interpretation of model parameters. Step 1. Although all three
- parameters were significantly different between the fructose- and glucose-labeled sucrose tracer
- curves, not all differences represented meaningful improvements in the fit of the breath curves to
- 256 the data. Indeed, for more than half of the participants, the SIC was lower when fixing $\pi \rho$ to be
- 257 the same for the two moieties. All curves could be reasonably fit with this assumption, as
- demonstrated in **Figure 3** where we plot the model fits to the fructose-labeled sucrose tracer and
- 259 the glucose-labeled sucrose tracer breath curves when $\pi\rho$ is the same for the two curves. This

result suggests that the gamma process (ρ), and not the exponential process ($\pi\rho$), is related to the transport and oxidation of fructose and glucose. Table S1 compares model fits for different assumptions for each participant.

Step 2. We compared the fit of the original, 3-parameter model to the uniformly labeled sucrose breath curve to the model that treats that curve as the average of curves for a fructose-labeled and a glucose-labeled sucrose tracer. We found that although the model accounting for the metabolism of the moieties separately could fit the data better, the functional improvement was negligible to minor and could be neglected. Table S2 compares the model fits for each participant, and the resulting fits to the data are plotted in Figure S1.

Step 3. Based on the results from Step 2, we applied the original model (Eqn 3) to the MLE experiments. Based on the results from Step 1 and 2, we investigated whether $\pi\rho$ could be held constant across each participant's three experiments. The SIC supported this assumption for 9 out of 16 curves, and all curves could be reasonably fit with this assumption, as demonstrated in **Figure** 4. This result suggests that the gamma process (ρ), and not the exponential process ($\pi\rho$), is related to sucrose hydrolysis. Table S3 compares model fits for different assumptions for each participant.

Development of a model-based 13 C-SBT diagnostic. Based on the above results, we proposed the value of ρ as a model-based 13 C-SBT diagnostic of intestinal SI activity. In **Figure 5**, we plot ROC curves to distinguish the 0 vs. 100 or 750 mg MLE curves and the 0 or 100 mg vs. 750 mg MLE curves for ρ and for cPDR90, peak PDRr, time to peak PDRr, and time to 50% cPDR. Our model-based statistic ρ had a comparable AUC (0.77) to cPDR90 (0.79) and time to peak PDRr (0.78) for distinguishing between the 0 mg and 100 or 750 mg breath curves. The peak PDRr and time to 50% cPDR (including only those curves with κ >0.5) statistics were poorer classifiers. Because the

curves associated with 0 or 100 mg and 750 mg were so different, all statistics were successful classifiers, with AUCs of 0.90 or greater.

Discussion

282

283

284

285

286

287

288

289

290

291

292

293

294

295

296

297

298

299

300

301

302

303

304

Stable isotope breath tests are non-invasive and have the potential to identify the functional changes in nutrient digestion and absorption caused by EED, a ubiquitous condition in areas with poor water, sanitation, and hygiene resources. Coupled with low food security and low diet quality and diversity, EED may lead to malnutrition and stunting in children. Unlike biopsies, which require surgical facilities and invoke ethical questions when sampling sub-clinical disease in children, breath sampling can be conducted in communities using collection bags or tubes. Samples have a long sample shelf-life and can be transported back to a central laboratory for analysis. Portable field analysis of ¹³CO₂ is also possible through infrared isotope spectroscopy, presenting potential opportunities to take the analytical laboratory into the community for nearly real-time analysis. Stable isotope breath tests can also be designed to interrogate the metabolism of a variety of nutrients. However, breath tests have not been widely adopted for this purpose, in part because of challenges in interpreting the breath curve output, especially when multiple biological processes may impact the signal. In this analysis, we used data from two sets of ¹³C-SBT experiments and a mechanistic model to connect breath test curve dynamics to underlying transport and metabolic processes, thereby improving the interpretation of ¹³C-SBT breath curves. In our previous work, we showed that breath test curves can be approximated by a gammadistributed (delay) process and an exponential process, along with a scaling factor for the fraction of tracer exhaled. Here, we demonstrated that both the transport and metabolism of the fructose and glucose moieties and the sucrose hydrolysis process are reflected in the gamma-distributed (delay) process. A model-based diagnostic of intestinal sucrase activity performed comparably to

conventional summary statistics when distinguishing between curves with and without an SI inhibitor. This work helps to advance the development and interpretation of the ¹³C-SBT, as well as other stable isotope breath tests for gut dysfunction.

Although we found that the model performed well for the uniformly labeled tracer in most cases, there is an inherent misspecification in the model when the fructose and glucose moieties are metabolized at different rates. Therefore, it is likely advisable to use a sucrose tracer with only one of the moieties labeled. Because fructose is sometimes metabolized so quickly, its dynamics are not always captured well by the standard 15 min data collection interval. Therefore, we would recommend the use of U-¹³C glucose in the ¹³C-SBT as a best practice when possible.

Conventional summary statistics of ¹³C breath curves do not fully take advantage of information contained by the shape of the breath curve and are not designed to reflect the underlying metabolic process of interest. Our work highlights the importance of identifying both which parts of the curve are impacted by the process of interest *and* which other processes impact the same part of the curve. If the process of interest is coupled with a highly variable process, the breath test itself may have relatively low diagnostic utility for all but the most extreme cases. For the ¹³C-SBT, we found that the transport to and processing in the liver (which would be different for the fructose and glucose moieties) affect the same parts of the breath test curve that sucrose hydrolysis does. Accordingly, the breath curves may look similar for those with certain types of liver dysfunction and for those with EED or related functional disorders, impacting the clinical interpretation of the results.

Conventional summary statistics have other limitations as well. We previously showed that cPDR90 is sensitive to the fraction of tracer exhaled, κ (17), which could vary as a function of

short-term physical activity as it is tied to V_{CO_2} (22,26). Time to peak PDRr, on the other hand, is not sensitive to κ , but may not be observed within reasonable testing periods for individuals with greater levels of gut dysfunction. Our model-based diagnostic, ρ , performed similarly to these summary measures in distinguishing between non-SI-inhibited and SI-inhibited breath curves and has the benefit of both being independent of κ and being able to be estimated for any length of breath curve, although the uncertainty associated with the estimate will be much greater if we do not observe some of the curve after the peak. In future work, we will assess the robustness of the diagnostic to the length of the testing period. Because of the limitations of any single diagnostic, we will also examine consensus classifiers that incorporate information from both conventional and model-based diagnostics.

The strengths of this work include the set of 13 C-SBT experiments targeting multiple processes underlying the tracer transport and metabolism, as well as the mechanistic framework. One limitation is that our participants were healthy adults in a high-income country. It is unclear how variable breath test curves are between settings (previous work showed systematic differences between breath test curves of adults in Glasgow and Zambia (20)) and between infants, children, and adults. Another limitation is that we did not have a direct measured of participant V_{CO_2} and used an approximation based on participant sex, body size, and sedentary physical activity level; fortunately, any misspecification in this quantity would only bias κ , the vertical scaling parameter. As we have previously described (17), the lack of dependence between V_{CO_2} and the model-based diagnostic is a strength of our approach. Another limitation is that we used biochemical inhibition to simulate gut dysfunction and did not have individuals with clinically diagnosed gastrointestinal disorders. On the other hand, the MLE experiments target intestinal sucrase activity precisely, so the risk of other metabolic changes impacting the breath results is very low. Accordingly, future

work is needed to establish the diagnostic potential and clinical utility of the ¹³C-SBT by comparing healthy individuals and individuals with clinically diagnosed dysfunction among the target population (e.g., children in a low-resource setting). Future work could also validate the mechanistic model (or add additional data to update it) by collecting serum samples to assess ¹³C dynamics in blood glucose and plasma bicarbonate.

Conclusion

We applied a recently developed mechanistic model to ¹³C-SBT breath curves to demonstrate how specific metabolic processes of sucrose hydrolysis and the transport and processing of the fructose and glucose moieties impact breath dynamics. We recommend the use of U-¹³C glucose in the ¹³C-SBT as a best practice to avoid potential misspecification caused by differential metabolism of fructose and glucose. Based on our work, we proposed a model-based diagnostic that performed comparably to conventional summary statistics while avoiding their practical limitations. While current summary approaches to interpreting ¹³C breath test successfully identify gross dysfunction in the gut, they may not be able to identify less severe dysfunction. Our diagnostic will enhance the interpretability of the ¹³C breath test curve in detecting a loss of SI activity leading to altered sucrose metabolism.

367 Acknowledgements

AFB, GOL, DJM designed the research; RJS, CAE, DJM conducted the research; AFB, HVW analyzed the data; AFB, GOL wrote the paper. AFB had primary responsibility for final content. All authors read and approved the final manuscript.

Data Availability: Data described in the manuscript, code book, and analytic code will be made publicly and freely available without restriction at https://doi.org/10.5281/zenodo.8387995

Funding: This project was funded through the International Atomic Energy Agency (IAEA) coordinated research projects E4.10.16 and E430336, United States National Science Foundation (NSF) grant DMS1853032, and United States National Institutes of Health (NIH) grant K01AI145080. The NSF and NIH were not involved in study design; collection, analysis, and interpretation of data; writing of the report. The IAEA was involved in study design of the data collection. The supporting sources did not have restrictions regarding publication.

Author Disclosures: None

References

- 1. Kurpad, A. V. The requirements of protein & amino acid during acute & chronic infections. *Indian J. Med. Res.* **124**, 129–48 (2006).
- 2. McCormick, B.J., Murray-Kolb, L.E., Lee, G.O., Schulze, K.J., Ross, A.C., Bauck, A.. et
- 371 al. Intestinal permeability and inflammation mediate the association between nutrient
- density of complementary foods and biochemical measures of micronutrient status in young
- 373 children: results from the MAL-ED study. *Am. J. Clin. Nutr.* **110**, 1015–1025 (2019).
- 374 3. Veitch, A. M., Kelly, P., Zulu, I. S., Segal, I. & Farthing, M. J. Tropical enteropathy: a T-
- 375 cell-mediated crypt hyperplastic enteropathy. Eur. J. Gastroenterol. Hepatol. 13, 1175–81
- 376 (2001).
- 4. Kelly, P., Ian, M., Crane, R., Zulu, I., Nickols, C., Feakins, R. et al. Responses of small
- 378 intestinal architecture and function over time to environmental factors in a tropical
- population. Am. J. Trop. Med. Hyg. 70, 412–9 (2004).
- 380 5. Owino, V., Ahmed, T., Freemark, M., Kelly, P., Loy, A., Manary, M. et al. Environmental

- Enteric Dysfunction and Growth Failure/Stunting in Global Child Health. *Pediatrics*.
- 382 **138**(6), e2016064 (2016).
- 383 6. United Nations Children's Fund (UNICEF), World Health Organization (WHO) &
- International Bank for Reconstruction and Development/The World Bank. Levels and
- trends in child malnutrition: UNICEF/WHO/World Bank Group joint child malnutrition
- *estimates: key findings of the 2023 edition.* (2023).
- 7. Crane, R. J., Jones, K. D. J. & Berkley, J. A. Environmental enteric dysfunction: An
- overview. *Food Nutr. Bull.* **36**, S76–S87 (2015).
- 8. Lee, G.O., Kosek, P., Lima, A.A., Singh, R., Yori, P.P., Olortegui, M.P. et al. Lactulose:
- Mannitol diagnostic test by HPLC and LC-MSMS platforms: Considerations for field
- studies of intestinal barrier function and environmental enteropathy. J. Pediatr.
- 392 *Gastroenterol. Nutr.* **59**, 544–550 (2014).
- 9. Denno, D. M., Tarr, P. I. & Nataro, J. P. Environmental Enteric Dysfunction: A Case
- Definition for Intervention Trials. Am. J. Trop. Med. Hyg. 97, 1643–1646 (2017).
- 395 10. Gupta, S. K., Chong, S. K. & Fitzgerald, J. F. Disaccharidase activities in children: normal
- values and comparison based on symptoms and histologic changes. J. Pediatr.
- 397 *Gastroenterol. Nutr.* **28**, 246–51 (1999).
- 398 11. Yu, J., Ordiz, M.I., Stauber, J., Shaikh, N., Trehan, I., Barnell, E. et al. Environmental
- Enteric Dysfunction Includes a Broad Spectrum of Inflammatory Responses and Epithelial
- Repair Processes. Cell. Mol. Gastroenterol. Hepatol. 2, 158-174.e1 (2016).
- 401 12. Ritchie BK, Brewster DR, Davidson GP, Tran CD, McNeil Y, Hawkes JS et al. 13C-
- 402 Sucrose Breath Test: Novel Use of a Noninvasive Biomarker of Environmental Gut Health.
- 403 *Pediatrics* **124**, 620–626 (2009).
- 13. Tran, C.D., Katsikeros, R., Manton, N., Krebs, N.F., Hambidge, K.M., Butler, R.N. et al.
- Zinc homeostasis and gut function in children with celiac disease. Am. J. Clin. Nutr. 94,
- 406 1026–1032 (2011).
- 14. Tran, C.D., Hawkes, J., Graham, R.D., Kitchen, J.L., Symonds, E.L., Davidson, G.P. et al.
- Zinc-Fortified Oral Rehydration Solution Improved Intestinal Permeability and Small
- Intestinal Mucosal Recovery. Clin. Pediatr. (Phila). 54, 676–682 (2015).
- 15. Skovbjerg, H., Sjöström, H. & Norén, O. Purification and Characterisation of Amphiphilic
- 411 Lactase/Phlorizin Hydrolase from Human Small Intestine. Eur. J. Biochem. 114, 653–661

- 412 (1981).
- 413 16. Mones, R. L. & Mercer, G. O. Ulcerative duodenitis in a child with celiac disease. J.
- 414 *Pediatr.* **158**, 857 (2011).
- 17. Brouwer, A.F., Lee, G.O., Schillinger, R.J., Edwards, C.A., Wyk, H.V., Yazbeck, R. et al.
- Mechanistic inference of the metabolic rates underlying 13 C breath test curves. J.
- 417 *Pharmacokinet. Pharmacodyn.* **0123456789**, (2023).
- 18. Oku, T., Yamada, M., Nakamura, M., Sadamori, N. & Nakamura, S. Inhibitory effects of
- extractives from leaves of Morus alba on human and rat small intestinal disaccharidase
- 420 activity. Br. J. Nutr. 95, 933–8 (2006).
- 421 19. Morrison, D. J., Dodson, B., Slater, C. & Preston, T. 13C natural abundance in the British
- diet: implications for 13C breath tests. Rapid Commun. Mass Spectrom. 14, 1321–1324
- 423 (2000).
- 20. Schillinger, R.J., Mwakamui, S., Mulenga, C., Tembo, M., Hodges, P., Besa, E. et al. 13C-
- sucrose breath test for the non-invasive assessment of environmental enteropathy in
- 426 Zambian adults. *Front. Med.* **9**, 1–13 (2022).
- 21. Slater, C., Preston, T. & Weaver, L. T. Stable isotopes and the international system of units.
- 428 Rapid Commun. Mass Spectrom. **15**, 1270–1273 (2001).
- 429 22. Amarri, S., Coward, W. A., Harding, M. & Weaver, L. T. Importance of measuring CO 2
- -production rate when using 13 C-breath tests to measure fat digestion . Br. J. Nutr. 79,
- 431 541–545 (1998).
- 432 23. Thondre, P. S., Lightowler, H., Ahlstrom, L. & Gallagher, A. Mulberry leaf extract
- improves glycaemic response and insulaemic response to sucrose in healthy subjects: results
- of a randomized, double blind, placebo-controlled study. Nutr. Metab. (Lond). 18, 41
- 435 (2021).
- 436 24. Ferraris, R. P., Choe, J. & Patel, C. R. Intestinal Absorption of Fructose. Annu. Rev. Nutr.
- **38**, 41–67 (2018).
- 25. Chong, M. F. F., Fielding, B. A. & Frayn, K. N. Mechanisms for the acute effect of fructose
- on postprandial lipemia. *Am. J. Clin. Nutr.* **85**, 1511–1520 (2007).
- 26. Zanconato, S., Cooper, D. M., Barstow, T. J. & Landaw, E. 13CO2 washout dynamics
- during intermittent exercise in children and adults. J. Appl. Physiol. 73, 2476–2482 (1992).

Table 1: Participant characteristics in the ¹³C-sucrose breath tests experiments.

	Experiment 1:	Experiment 2:	
	Sucrose moiety labeling	Sucrase-isomaltase inhibition	
N	19	16	
Age, mean (sd)	22.9 (4.4)	24.2 (5.0)	
Sex ratio, female:male	10:9	8:8	
BMI, mean (sd), kg/m ²	22.1 (3.6)	24.5 (5.2)	

Figure Legends

442

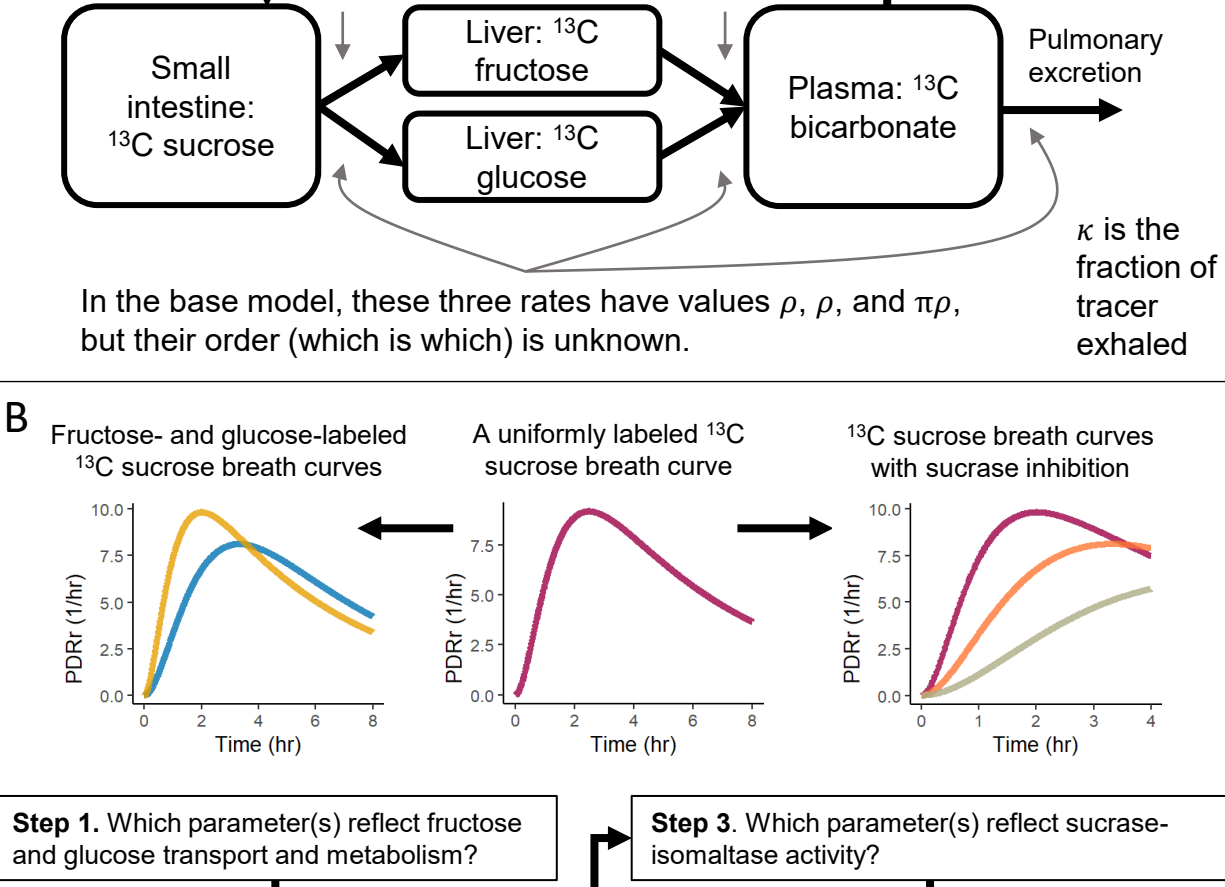
- Figure 1: A: Schematic of the mechanistic model of the ¹³C sucrose breath test, accounting for the possibility of separate rates of fructose and glucose transport and metabolism. B: Schematic of the analysis plan.
- Figure 2: Comparison of three mechanistic model parameters between ¹³C-sucrose breath test experiments for (top row) a fructose-labeled sucrose tracer and a glucose-labeled sucrose tracer and (bottom row) uniformly labeled sucrose tracer with 0, 100, and 750mg of mulberry leaf extract

(MLE). Note that the parameters πρ and κ were not identifiable for many of the breath curves with
 750 mg MLE, and so those values should be treated with caution.

Figure 3: Individual ¹³C-sucrose breath test curves for sucrose with a fructose-labeled moiety and sucrose with a glucose-labeled moiety (points) and their associated best-fit mechanistic models (lines) using the assumption that the exponential process ($\pi\rho$) is the same for both of each participant's curves. The y-axis is allowed to vary between plots to enhance readability.

Figure 4: Individual ¹³C-sucrose breath test curves for the set of experiments with increasing doses of mulberry leaf extract and their associated best-fit mechanistic models (lines) using the assumption that the exponential process is the same for both of each participant's curves. The y-axis is allowed to vary between plots to enhance readability.

Figure 5: Receiver operator curves (ROC) for classifying breath test curves by the dose of mulberry leaf extract, a sucrase-isomaltase inhibitor intended to approximate gut dysfunction. The four rows use cumulative percent dose recovered by 90 minutes (cPDR90), time to peak percent dose recovery rate (PDRr), peak PDRr, and the model-based diagnostic ρ. The left column gives the ROCs for 0 vs 100 mg dose and the right column gives the ROCs for 0 vs 750 mg. The optimal threshold (OT) and area under the curve (AUC) are given for each ROC. The time to 50% cPDR comparisons include only those curves where κ was estimated to be at least 0.5



Metabolism

of moieties

Sucrose hydrolyzed

into moieties

Small liquid

tracer ingested

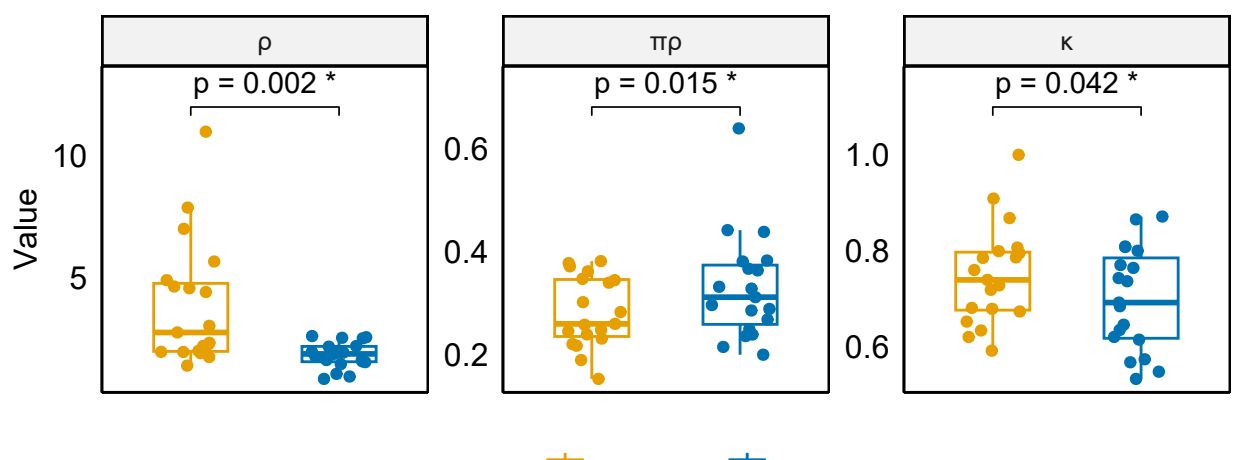
Sequestration and

urinary excretion

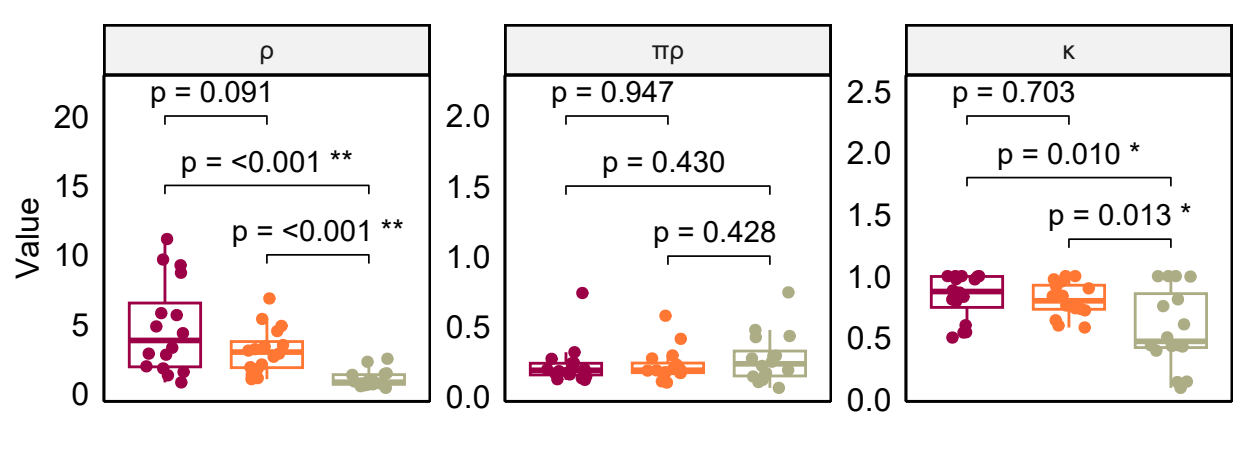
and glucose transport and metabolism?

Step 2. How much does accounting for differences in fructose and glucose transport improve the model?

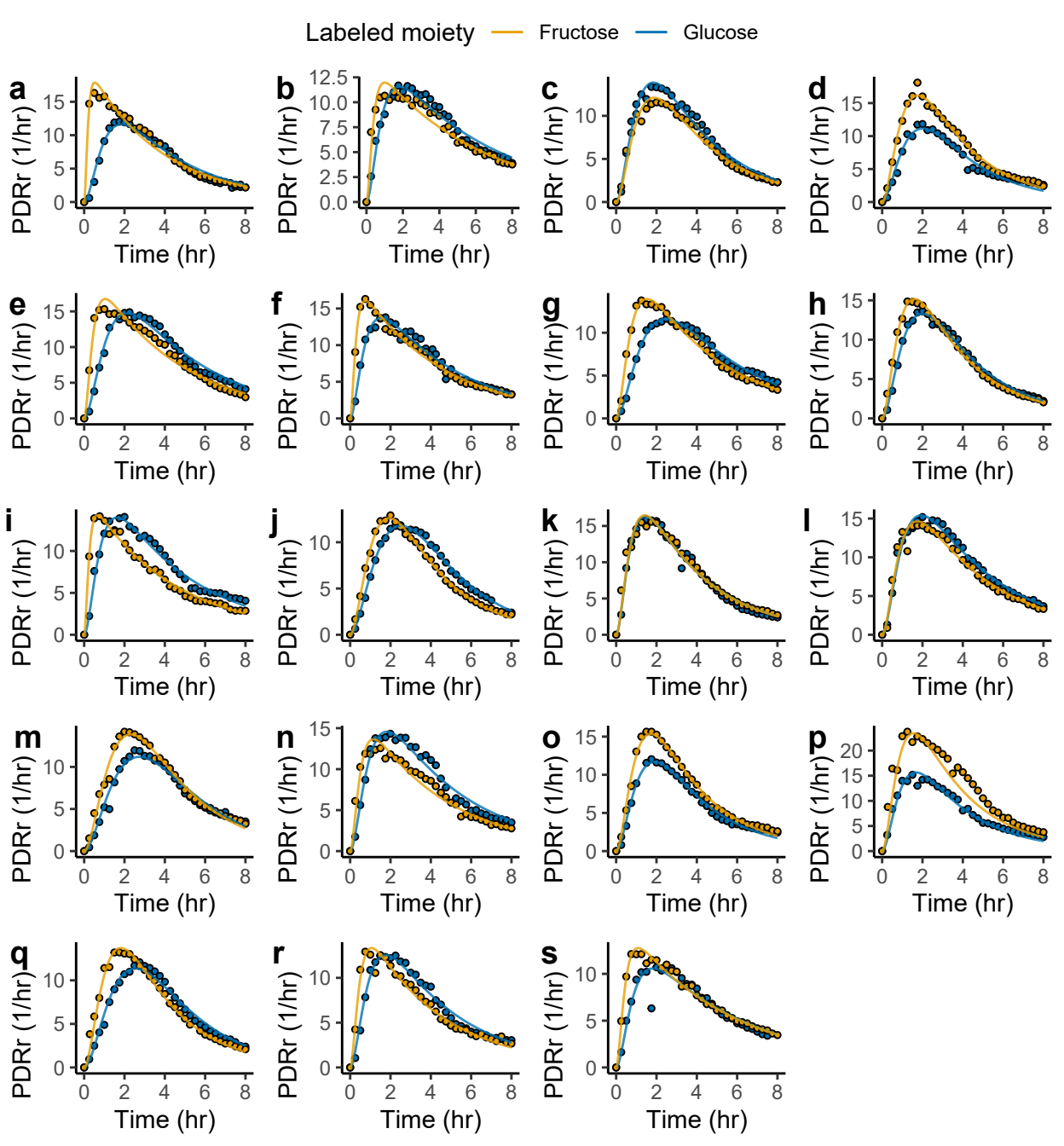
Application. How does a model-based diagnostic compare to conventional summary statistics for distinguishing between degrees of sucrase-isomaltase inhibition?

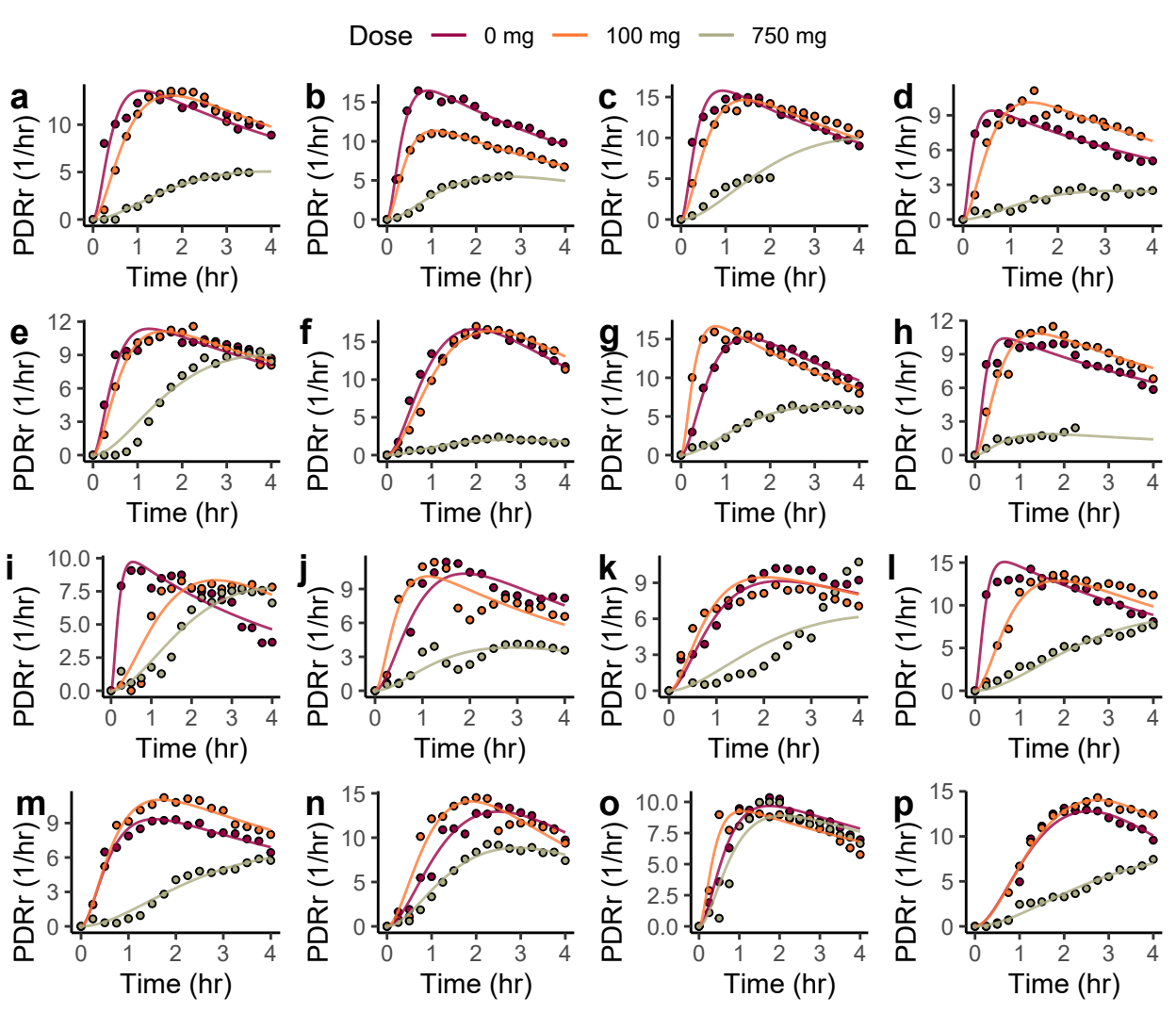


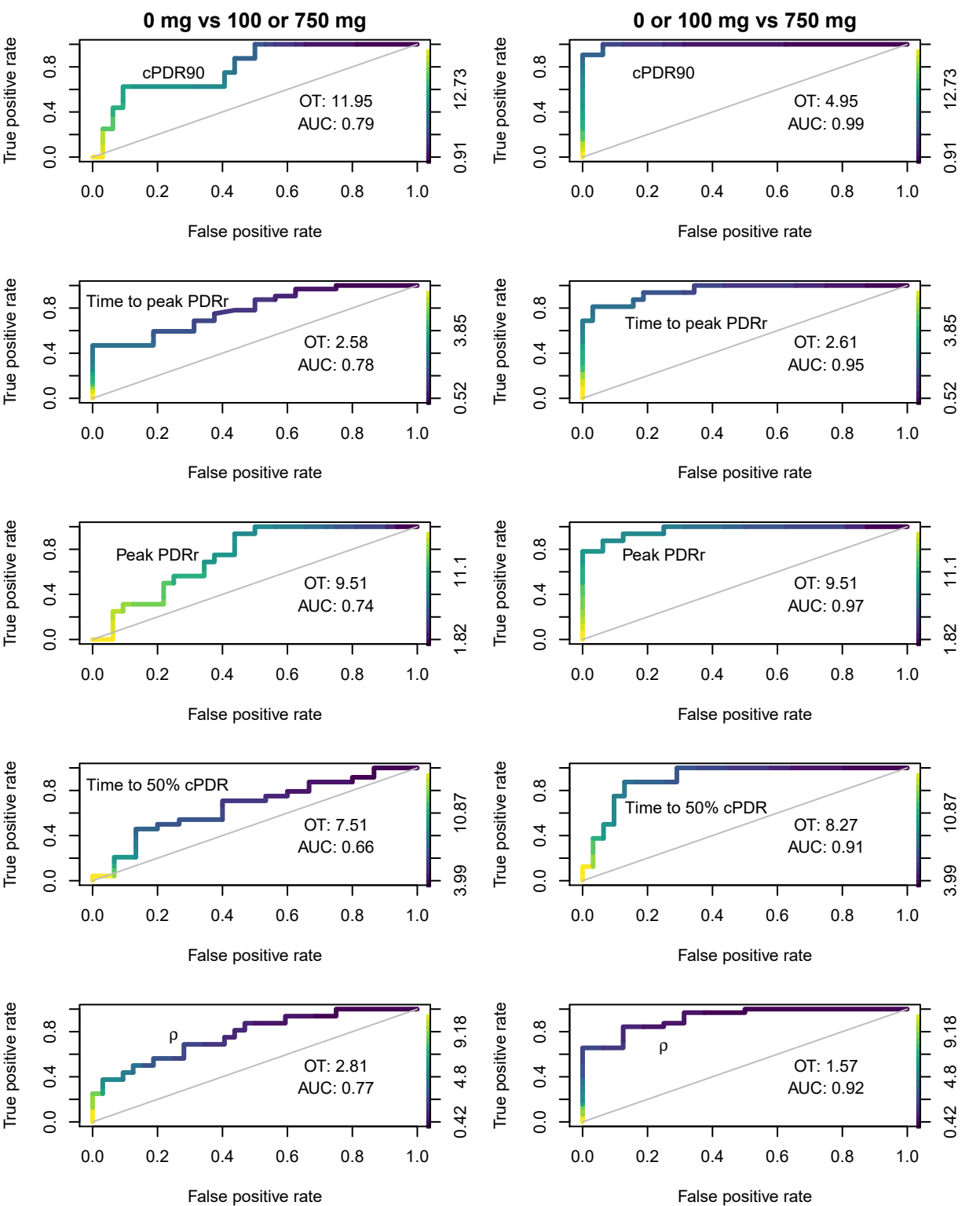
Label Fructose Glucose



Label 🗭 0 🔖 100 🔖 750







Supplemental material for Connecting 13C-sucrose breath test curve dynamics to underlying metabolic processes: exploratory experiments and development of a model-based 13C-sucrose breath test diagnostic for gut function disorders characterized by a loss of sucrase-isomaltase enzymatic activity by Brouwer et al.

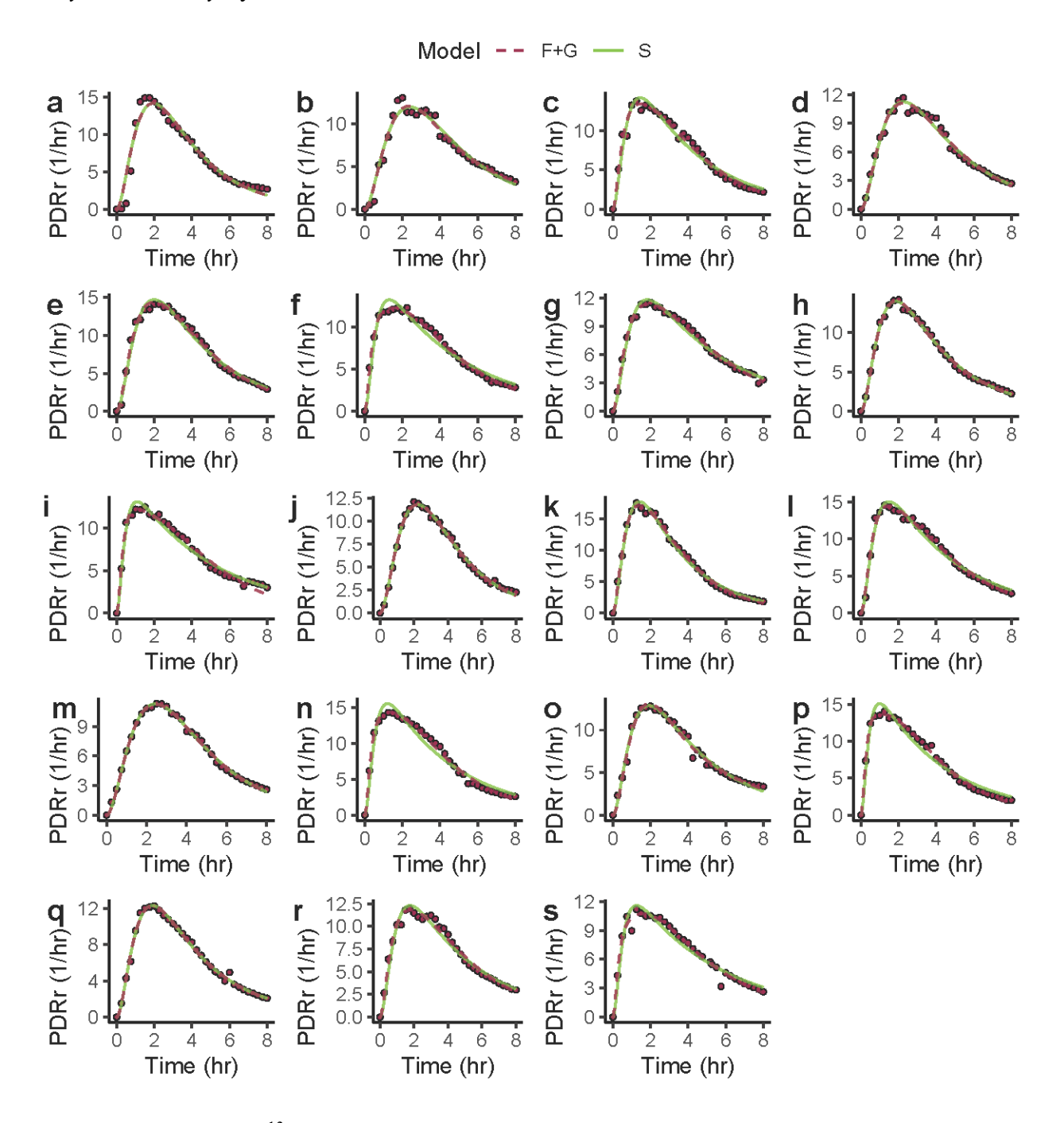


Figure S1: Individual ¹³C-sucrose breath test curves uniformly labeled sucrose (points) and their associated best-fit mechanistic models (lines) using the three-parameter model (S) and the four-parameter model treating the curve as the sum of fructose- and glucose-labeled tracer curves (F+G). The y-axis is allowed to vary between plots to enhance readability.

Table S1: Comparison of SIC model fits to the fructose-labeled and glucose-labeled sucrose breath test curves as assumptions are varied. The lowest SIC value for each participant is highlighted. F subscripts denote parameters for the model fit to the fructose-labeled sucrose breath test curve, and the G subscripts denote parameters for the model fit to the fructose-labeled sucrose breath test curve.

	Model number	1	2	3	4	5	6	7
	Parameters and	$\rho_F, \rho_G,$	$ \rho_F = \rho_G, $	$ \rho_F = \rho_G $	$\rho_F, \rho_G,$	$\rho_F, \rho_G,$	$ \rho_F = \rho_G, $	$\rho_F, \rho_G,$
	assumptions	$\pi_F \rho_F = \pi_G \rho_G,$	$\pi_F \rho_F$, $\pi_G \rho_G$,	$\pi_F \rho_F = \pi_G \rho_G,$	$\pi_F \rho_F$, $\pi_G \rho_G$,	$\pi_F \rho_F = \pi_G \rho_G,$	$\pi_F \rho_F, \pi_G \rho_G,$	$\pi_F \rho_F, \pi_G \rho_G,$
	•	$\kappa_F = \kappa_G$	$\kappa_F = \kappa_G$	κ_F, κ_G	$\kappa_F = \kappa_G$	κ_F, κ_G	κ_F, κ_G	κ_F, κ_G
Participant								
SFG1		230.73	727.48	893.59	222.74	160.27	729.99	125.37
SFG2		170.59	260.69	256.12	147.72	158.49	245.30	149.18
SFG3		184.10	151.61	133.71	146.39	137.49	136.54	140.39
SFG4		436.66	241.00	161.59	231.43	138.45	144.91	142.49
SFG5		189.06	603.38	651.79	148.30	170.76	512.29	149.11
SFG6		122.74	345.38	393.84	126.84	126.54	327.55	128.50
SFG7		88.82	221.56	318.17	91.98	91.70	182.21	95.88
SFG8		89.64	126.76	165.17	93.64	90.09	129.50	91.41
SFG9		203.69	512.74	464.04	147.12	110.06	338.02	113.73
SFG10		90.52	159.72	198.33	74.33	75.66	112.88	77.09
SFG11		174.89	174.55	175.23	175.79	179.01	176.35	172.50
SFG12		189.44	190.33	167.68	163.95	156.51	164.37	160.41
SFG13		166.45	151.82	194.16	152.31	132.43	151.78	133.33
SFG14		303.75	376.34	303.45	156.30	169.38	280.82	153.51
SFG15		252.41	158.12	110.36	155.78	99.81	103.79	103.89
SFG16		1808.72	937.69	646.73	824.37	641.57	614.39	611.47
SFG17		106.60	197.53	303.18	106.04	110.71	187.35	99.55
SFG18		147.87	292.45	292.71	117.84	130.97	259.56	121.91
SFG19		175.31	229.85	259.14	169.81	162.21	230.82	163.83

Table S2: Comparison of SIC model fits to the uniformly labeled sucrose breath test curves as assumptions are varied. The lowest SIC value for each participant is highlighted. F subscripts denote parameters for the model fit to the fructose-labeled sucrose breath test curve, and the G subscripts denote parameters for the model fit to the fructose-labeled sucrose breath test curve. The SF subscripts denote parameters for the model fit to the fructose moiety of the uniformly labeled sucrose breath test curve, and the SG subscripts denote parameters for the glucose moiety of the uniformly labeled sucrose breath test curve.

	Model number	1	2
	Parameters and	ρ_{SF}, ρ_{SG}	$ \rho_{SF} = \rho_{SG} $
	assumptions	$\pi_{SF}\rho_{SF}=\pi_{SG}\rho_{SG},$	$\pi_{SF}\rho_{SF}=\pi_{SG}\rho_{SG},$
		$\kappa_{SF} = \kappa_{SG}$	$\kappa_{SF} = \kappa_{SG}$
Participant			
SFG1		154.27	154.27
SFG2		83.37	88.89
SFG3		66.79	105.15
SFG4		54.98	56.50
SFG5		55.48	65.98
SFG6		42.75	87.26
SFG7		41.42	52.76
SFG8		43.75	43.18
SFG9		56.86	69.51
SFG10		42.43	42.43
SFG11		51.06	64.41
SFG12		56.12	74.29
SFG13		40.49	40.49
SFG14		49.21	118.34
SFG15		56.23	58.08
SFG16		43.70	99.84
SFG17		45.68	45.69
SFG18		52.46	72.35
SFG19		54.66	86.55

Table S3: Comparison of SIC model fits to the sucrase-isomaltase inhibition experiment breath test curves as assumptions are varied. The lowest SIC value for each participant is highlighted. Subscripts R1, R2, and R3 denote the curves for the 0 mg, 100 mg, and 750 mg experiments, respectively.

	Model number	1	2
	Parameters and assumptions	$ ho_{R1}, ho_{R2}, ho_{R3} ho_{R3} ho_{R1}, \pi ho_{R2}, \pi ho_{R3} ho_{R3} ho_{R1}, \kappa_{R2}, \kappa_{R3}$	$ \rho_{R1}, \rho_{R2}, \rho_{R3} \pi \rho_{R1} = \pi \rho_{R2} = \pi \rho_{R3} \kappa_{R1}, \kappa_{R2}, \kappa_{R3} $
Participant		10K1) 10K2) 10K3	11,11,11,11,11,11
MLE1		139.88	140.92
MLE2		83.97	77.08
MLE3		130.58	148.95
MLE4		94.63	87.65
MLE5		138.68	141.30
MLE6		122.24	133.46
MLE7		102.47	95.46
MLE8		115.01	110.51
MLE9		194.20	187.09
MLE10		242.56	241.18
MLE11		226.27	358.54
MLE12		124.43	170.82
MLE13		101.23	94.85
MLE14		221.99	214.83
MLE15		156.02	173.07
MLE16		200.74	188.83